

Lawrence Berkeley National Laboratory

LBL Publications

Title

Design and Synthesis of Annulated Benzothiadiazoles via Dithiolate Formation for Ambipolar Organic Semiconductors

Permalink

<https://escholarship.org/uc/item/9qj8g2rh>

Journal

ACS Applied Materials & Interfaces, 12(47)

ISSN

1944-8244

Authors

Kolaczkowski, Matthew A

Garzón-Ruiz, Andrés

Patel, Akash

et al.

Publication Date

2020-11-25

DOI

10.1021/acsami.0c16056

Peer reviewed

Design and Synthesis of Annulated Benzothiadiazoles via Dithiolate Formation for Ambipolar Organic Semiconductors

Matthew A. Kolaczkowski,^{a,b} Andrés Garzón-Ruiz,^c Akash Patel,^{a,b} Zhiyuan Zhao,^d Yunlong Guo,^d Amparo Navarro,^{*e} Yi Liu^{*a}

^aThe Molecular Foundry, Lawrence Berkeley National Laboratory, Berkeley, California 94720, USA

^bDepartment of Chemistry, University of California, Berkeley, California 94720, USA

^cDepartment of Physical Chemistry, Faculty of Pharmacy, Universidad de Castilla-La Mancha, Cronista Francisco Ballesteros Gómez, Albacete 02071, Spain

^dInstitute of Chemistry, Chinese Academy of Sciences, Beijing 100190, P. R. China

^eDepartment of Physical and Analytical Chemistry, Faculty of Experimental Sciences, Universidad de Jaén, Campus Las Lagunillas, Jaén 23071, Spain

Corresponding authors: yliu@lbl.gov, anavarro@ujaen.es

Abstract:

Substituted 2,1,3-benzothiadiazole (BTD) is a widely used electron acceptor unit for functional organic semiconductors. Difluorination or annulation on the 5,6-position of the benzene ring are amongst the most adapted chemical modifications to tune the electronic properties, though each sees its own limitations in regulating the frontier orbital levels. Herein a hitherto unreported 5,6-annulated BTD acceptor, denoted as ssBTD, is designed and synthesized by incorporating an electron withdrawing 2-(1,3-dithiol-2-ylidene)malonitrile moiety via aromatic nucleophilic substitution of the 5,6-difluoroBTD (ffBTD) precursor. Unlike the other reported BTD annulation strategies, this modification leads to the simultaneous decrease of both frontier orbital energies, a welcoming feature for photovoltaic applications. Incorporation of ssBTD in conjugated polymers results in materials boasting broad light absorption, dramatic solvatochromic and thermochromic responses (>100 nm shift and a bandgap difference of ~0.28 eV), and improved crystallinity in the solid state. Such physical properties are in accordance with the combined electron withdrawing effect and

significantly increased polarity associated with the ssBTD unit, as revealed by detailed theoretical studies. Furthermore, the thiolated ssBTD imbues the polymer with ambipolar charge transport property, in contrast to fBTD based polymer which transports hole only. While the low mobilities (10^{-4} to 10^{-5} $\text{cm}^2 \text{V}^{-1} \text{s}^{-1}$) could be further optimized, the detailed studies validate that the thioannulated BTD is a versatile electron accepting unit for the design of functional stimuli-responsive optoelectronic materials.

Keywords: ambipolar, benzothiadiazole, dithiolate annulation, electron acceptor, organic semiconductor, solvatochromic

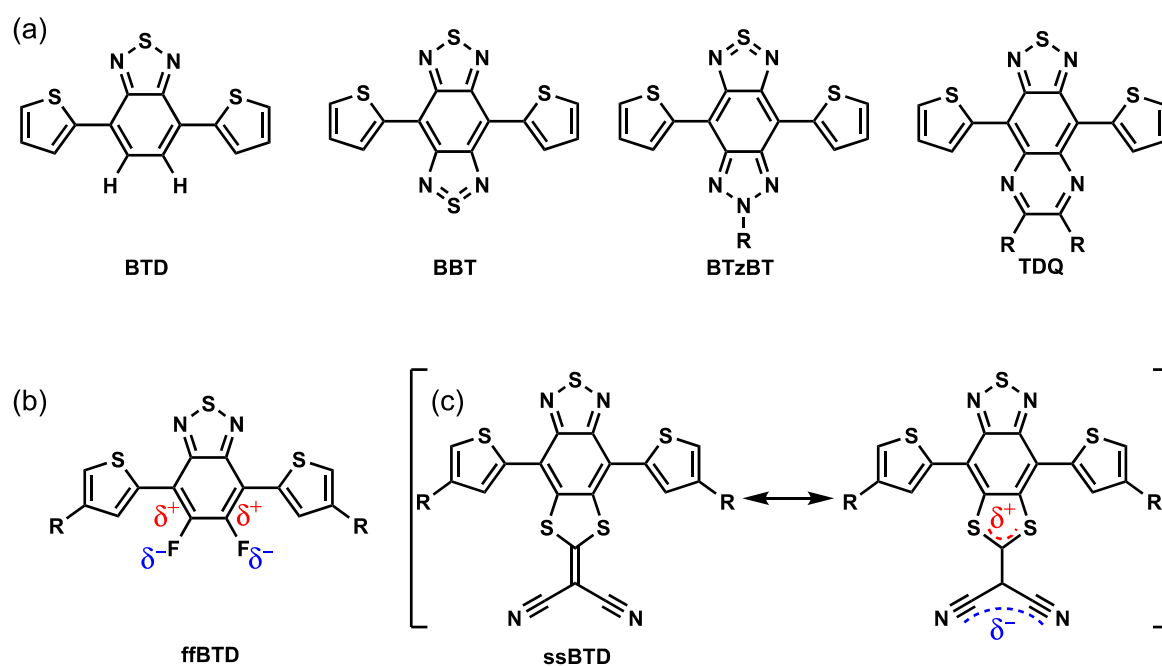
Introduction

Synthetic efforts to increase light absorption, tune energy levels, as well as alter solid state packing and charge transport have been increasingly fruitful in boosting the efficiency of organic photonic devices.¹ The ability to effectively tune optical and electronic properties benefits greatly from a modular “donor-acceptor” (DA) approach, which involves covalent coupling of electron-rich donors and electron-poor acceptors either directly or through a π -conjugation bridge.²⁻⁹ This approach grants control over electronic properties since the energy levels of the donor-acceptor materials are generally dependent on the highest occupied molecular orbital (HOMO) energy level of the donor and the lowest occupied molecular orbital (LUMO) energy level of the acceptor. While the availability of a wide range of electroactive building blocks has greatly driven the forefront of organic semiconductor applications in organic photovoltaics (OPVs),¹⁰⁻¹³ organic field effect transistors (OFETs),^{2-9,14} organic light emitting diodes (OLEDs),^{15,16} and electrochromic devices,¹⁷⁻¹⁹ electron acceptors are relatively underdeveloped compared to electron donors and have remained an active research direction.²⁰

One of the most studied electron acceptors is 2,1,3-benzothiadiazole (BTD),^{21,22} which is widely used in small molecules, oligomers and conjugated polymers. Although innately a strong acceptor, great lengths have been taken to increase and alter the withdrawing effect of the BTD system. By substituting the 5- and 6-positions, the electronics of BTD can be altered while maintaining the 4- and 7- positions for coupling to electron-rich donors. The most common substitutions are through heteroannulation^{22,23} as in [1,2,5]thiadiazolo[3,4-g]quinoxaline (TDQ),^{24,25} benzo[1,2-c:4,5-c']bis[1,2,5]thiadiazole (BBT),^{21,26} and benzo(triazole-thiadiazole) (BTzTD),^{27,28} or attachment of electron withdrawing fluorides as in difluoro-substituted BTD (ffBTD)²⁹⁻³⁸ and dicyano-substituted BTD.³⁹⁻⁴¹ For these annulated TDQ and BBT systems, while annulation effectively lowers the LUMO energy to give stronger electron acceptors, it simultaneously raises the HOMO energies, which is disadvantageous for their incorporation in electron donor materials for OPVs as it is correlated to a decrease of open-circuit voltage.²²

Herein we devised a new 5,6-annulated BTD ring system using aromatic nucleophilic substitution (S_NAr) to introduce an electron withdrawing 2-(1,3-dithiol-2-ylidene)malonitrile group using the common ffBTD as a precursor. Early examples using dithiolates for the annulated electron acceptors were demonstrated in the fusion of 2-(1,3-dithiol-2-ylidene)malonitrile with quinones⁴² or naphthalene diimide (NDI) derivatives.⁴³⁻⁴⁶ The fluorine atoms in ffBTD are particularly activated as leaving groups for S_NAr by the electron deficient BTD unit, and as a result they are readily displaced by 2,2-dicyanoethene-1,1-dithiolate to give the thiolated BTD, denoted as ssBTD. While the fluorides in ffBTD effectively lower both HOMO and LUMO energy levels relative to the parent BTD via an induction effect, the dithiolate adduct with 2,2-dicyanoethene-1,1-dithiolate in ssBTD provides a similar withdrawing effect through resonance (**Scheme 1**). This withdrawing effect can be visualized through a zwitterionic resonance form where the anion is stabilized by two

withdrawing groups, while the cation is stabilized by neighboring electron rich thioethers. This annulation has the added benefit of locking the electron accepting subunit into a planar configuration with the rest of the molecule, enforcing strong orbital overlap and conjugation. The successful synthesis of the ssBTD unit permits detailed assessment of such an annulation effect, in direct comparison to the unsubstituted BTD and the ffBTD precursor. Incorporation of the ssBTD unit in conjugated polymers further allows us to evaluate how the subtle interplay between electronic and steric effects alter key materials properties, such as solvatochromism and thermochromism, thin film morphology, and charge carrier transport properties.

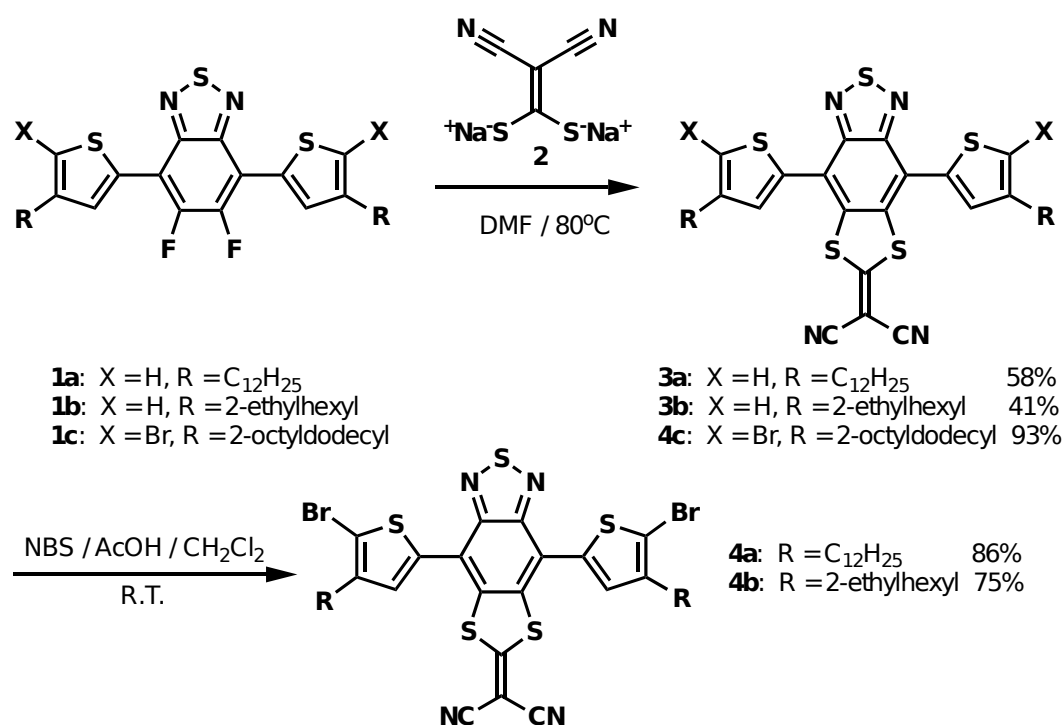


Scheme 1. (a) List of BTD and annulated BTD derivatives. Illustration of the electron withdrawing effects in BTDs: (b) induction effect by fluorine in ffBTD, and (c) resonance effect by the malononitrile dithiolate group in ssBTD.

Results and Discussion

Materials Synthesis. In order to control for solubility, ffBTD derivatives **1a** and **1b** were utilized which incorporated thiophene groups with linear $n\text{-C}_{12}\text{H}_{25}$ and a branched 2-

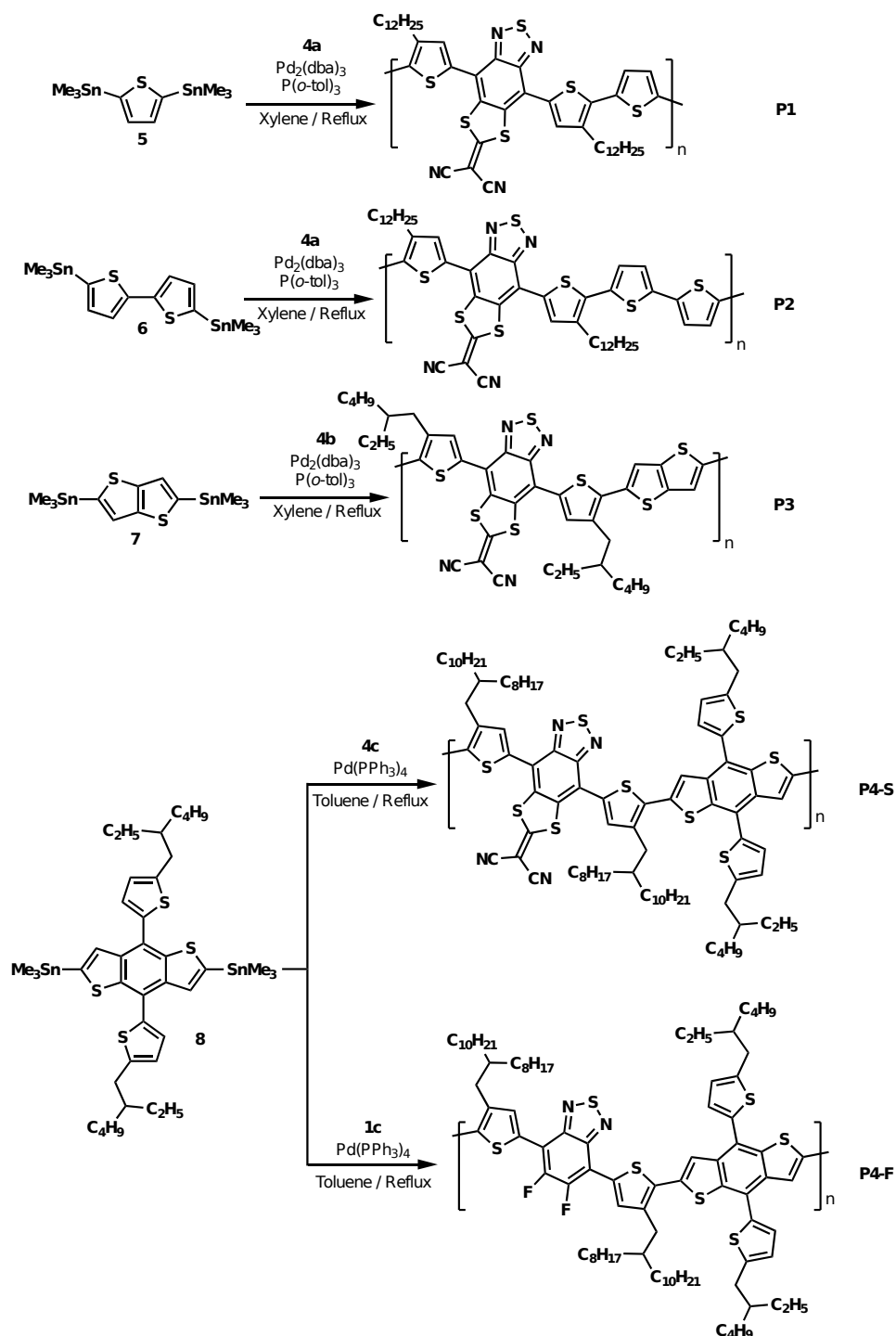
ethylhexyl (2-EH) alkyl substituents, respectively (**Scheme 2**). These compounds were reacted with disodium 2,2-dicyanoethelene-1,1-dithiolate (**2**) in DMF at 80 °C to provide the desired products **3a** and **3b** which were isolated in moderate yields. To insert functional handles, the compounds underwent clean bromination to **4a** and **4b**. In the reaction of **2** with the ffBTD **1c**, which bears a longer 2-octyldodecyl alkyl chain and a bromide in the flanking thiophene unit, the desired product **4c** was obtained in excellent yield with the thiolate substitution occurred selectively at the fluorinated positions over the less activated brominated positions.



Scheme 2. Synthesis of ssBTD derivatives via S_NAr reaction with ffBTDs.

A series of conjugated polymers were synthesized by subjecting the bromides **4a-c** to Pd-catalyzed cross-coupling reactions with a variety of electron-rich bis(stannane)s (**Scheme 3**). Polymers **P1** and **P2** were obtained from the reactions between monomer **4a** and thiophene bis(stannane) (**5**) and bithiophene bis(stannane) (**6**), respectively. Such polymers have low solubilities, presumably due to strong aggregation between polymer chains. Copolymerization between the branched 2-ethylhexyl chain-bearing **4b** and thienothiophene bis(stannane) (**7**)

gave polymer **P3** with slightly increased solubility, though for all three polymers the solubility is still quite limited which significantly hinders the solution processability and prevents their integration in electronic devices.



Scheme 3. Synthesis of conjugated polymers based on ssBTD derivatives **4a-c** and a control polymer based on fBTD **1c**.

To ensure better solubility, the ssBTD monomer **4c** with pendant 2-octyldecyl chains on the thiophene units was cross-coupled with the 2-ethylhexylthiophene-substituted benzodithiophene (BDT) bis(stannate) **8** to give polymer **P4-S**. For comparison, an analogous polymer **P4-F** was also synthesized from copolymerizing the ffBTD **1c** with the same BDT monomer **8**. The introduction of branched alkyl chains on both the donor and acceptor monomeric units resulted in vastly improved solubility for polymers **P4-S** and **P4-F** relative to polymers **P1-P3**, as verified by the attempted Soxhlet fractionation. Only a small amount of soluble species could be fractionated from polymers **P1-P3** using a variety of common solvents, with the remainder being insoluble even in high boiling point solvents such as chlorobenzene and *o*-dichlorobenzene (ODCB). In stark contrast, **P4-F** was soluble in pure hexane and in the case of **P4-S** two main fractions were obtained from hexane and THF Soxhlet extraction.

Molecular weight analysis of these polymers was carried out using high temperature size exclusion chromatography (SEC) using trichlorobenzene as the eluent and polystyrene as the standard (see **Table 1**). The Soxhlet fraction from **P1** had the highest number-averaged molecular weight (M_n) amongst all, while the low solubility of **P2** prevented characterization even in the high temperature environment. Polymer **P3** was determined to be composed of small oligomers, as characterized by the lowest M_n and a low polydispersity. The more soluble **P4-S** and **P4-F** had comparatively high molecular weights. The THF fraction of **P4-S** has slightly higher M_n and polydispersity than that of the hexane fraction, but both had higher molecular weights and polydispersities than **P4-F**. Additional thermogravimetric analysis (TGA) of **P4-S** revealed good thermal stability, with a thermal decomposition onset temperature of 235 °C (**Figure S1**). Differential scanning calorimetry (DSC) studies indicated no phase change within this range.

Table 1. Molecular weight distribution of substituted benzothiadiazole polymers.^{a)}

	Polymer	Mn	Mw	polydispersity	
^{a)} Molecular weight measured at 180 °C in polystyrene	P1	2.02×10 ⁴	4.16×10 ⁴	2.06	weight measured
	P2	- ^{d)}	- ^{d)}	- ^{d)}	reference to
	P3	0.53×10 ⁴	0.60×10 ⁴	1.13	standards;
^{b)} extracted by	P4-F^{b)}	1.02×10 ⁴	2.00×10 ⁴	1.95	hexane;
^{c)} extracted by	P4-S-hex^{b)}	1.37×10 ⁴	3.56×10 ⁴	2.59	THF; ^{d)} not
determined due	P4-S-THF^{c)}	1.67×10 ⁴	4.96×10 ⁴	2.98	to low solubility.

Optical and Electrochemical Characterizations. To determine the effect of substitution, the optical and electrochemical properties of ffBTD **1a** and the thiolated ssBTDs **3a-b** were evaluated relative to the unsubstituted parent benzothiadiazole **S1** (**Figure 1** and **Table 2**).

Using DFT calculations, the frontier molecular orbitals and the relative energy level of these small molecules were compared in **Figure 1b** (see Supporting Information for details). UV-Vis absorption spectra indicated that both forms of substitutions on BTD resulted in slight blue shift of the absorption maximum at the longest wavelength compared to the hydrogen substituted **S1** (**Figure 1c**). These experimental results were confirmed through TD-ωB97xD/6-31G** calculations (**Figure 1d** and **Table S1**). The absorption maximum at the longest wavelength was calculated for **S1** at 409 nm and corresponded to a HOMO→LUMO transition, which was closely followed by the HOMO→LUMO transition calculated for **1a** at 408 nm. The dithiolation also introduced the appearance of a new and intense absorption band around 400 nm, resulting in an overall wider spectral coverage than **1a** or **S1**. Two electronic transitions were calculated at 327 nm (HOMO-1→LUMO) and 382 nm (HOMO→LUMO) for **3a** and assigned to the absorption maximum band and its lower-energy shoulder.

Figure 1. (a) Chemical structures and (b) frontier orbital plots of BTD **S1**, fBTD **1a** and ssBTD **3a** (isocontour plots (0.02 au)). (c) Experimental and (d) calculated UV-vis spectra for these molecules (plotted with a peak half-width at half-height of 0.25 eV). The vertical bars correspond to the oscillator strengths of the calculated electronic transitions. (e) cyclic voltammetry and (f) estimated frontier orbital energy levels of these small molecules based on electrochemical studies. Solvent: CHCl₃.

Cyclic voltammetry (CV) studies provided more information to estimate and compare the frontier orbital energy levels of these **BTD** derivatives (**Figure 1e** and **1f**). Both **1a** and **3a** displayed irreversible oxidation and reduction peaks during the CV scan, from which a larger oxidation onset potential and a smaller reduction onset potential than **S1** were observed, showing that both HOMO and LUMO levels were lowered compared to that of **S1**. Compound **3a** had the lowest HOMO level and a LUMO only slightly higher relative to **1a**. In general, similar conclusions were obtained from DFT calculations although both the lowest HOMO and LUMO levels were predicted for **3a** (**Figure 1b** and **Table S2**).

Table 2. Summary of the optical and electrochemical properties of BTD-based small molecules.

a)absorptio	Compd	UV-Vis			Cyclic Voltammetry		n peak of
		$\lambda_{max,1}^{a)}$ (nm)	$\lambda_{max,onset}$ (nm)	$\lambda_{max,2}^{b)}$ (nm)	E_{HOMO} (eV)	E_{LUMO} (eV)	
the lowest	S1	458	527	312	-5.40	-3.11	energy;
b)absorptio	1a	440	503	310	-5.61	-3.52	n peak of
	3a	455	511	404	-5.83	-3.43	

the second lowest energy.

Solvatochromic and Thermochromic Effects. Optical studies of the **BTD** polymers revealed apparent color changes in response to different solvents and temperatures, indicating strong solvatochromic and thermochromic effects (**Table 3**). In pure hexane, **P4-S** displayed a

green color and an optical onset of around 743 nm, corresponding to a band gap of 1.66 eV. When the solvent is switched to CHCl₃, the color changes to pinkish red and the optical onset of the solution absorption spectrum blue shifted to 639 nm, corresponding to an almost 100 nm negative solvatochromic shift and a band gap increase of 0.28 eV (**Figure 2**). Polymer **P4-F** showed a similar but less pronounced solvatochromic shift of the absorption onset from 698 nm in hexane to 616 nm in CHCl₃, showing a corresponding color change from blue to purple and a band gap increase of ~0.24 eV. Though CHCl₃ tends to disentangle the polymer chains, **P4-F** appears to remain partially aggregated in CHCl₃ at room temperature, which shows a color change from purple to light pink when heated to 55 °C. On the other hand, **P4-S** shows no noticeable color change when the CHCl₃ solution is heated to 55 °C, suggesting that it is almost molecularly dissolved at room temperature.

Table 3. Summary of the optoelectronic properties of the polymers.

Compd	UV-Vis Aggregated		UV-Vis Disaggregated ^{a)}		Cyclic Voltammetry		
	λ_{onset} (nm)	E_g^{opt} (eV)	λ_{onset} (nm)	E_g^{opt} (eV)	E_{HOMO} (eV)	E_{LUMO} (eV)	E_g^{Elec} (eV)
P1	817 ^{b)}	1.52	800 ^{d)}	1.55 ^{d)}	-5.35	-3.61	1.74
P2	785 ^{b)}	1.58	662	1.87	-5.30	-3.40	1.90
P3	822 ^{b)}	1.51	682	1.82	-5.39	-3.54	1.85
P4-F	698 ^{c)}	1.77	616	2.01	-5.74	-3.66	2.08
P4-S	743 ^{c)}	1.66	639	1.94	-5.50	-3.59	1.92

^{a)}determined from chloroform solution at 55 °C; ^{b)}determined from hexane solution; ^{c)}determined from 1:1 hexane/chloroform solution; ^{d)}Not fully disaggregated, even at elevated temperatures.

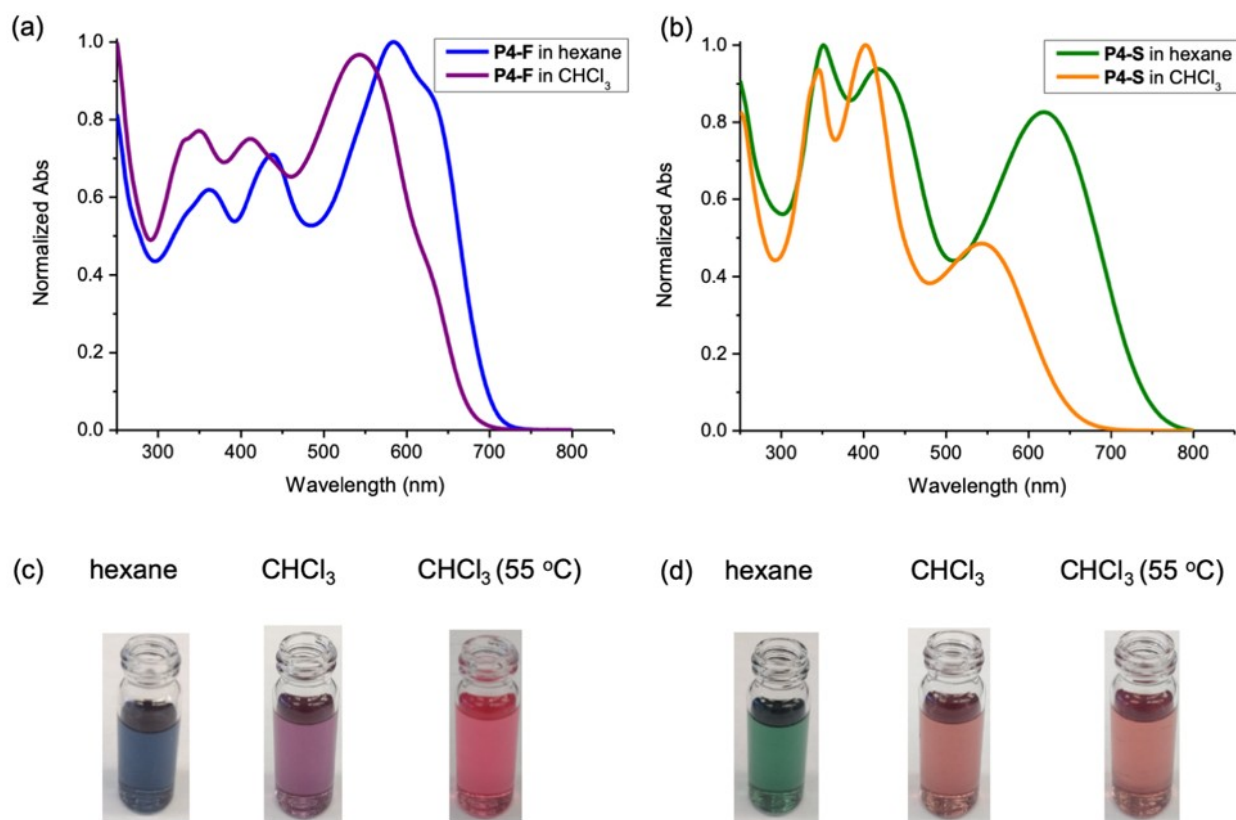


Figure 2. UV-Vis spectra of (a) **P4-F** and (b) **P4-S** in CHCl₃ and hexane. Pictures in (c) and (d) displayed the color changes of the two polymers in different solvents and in hot CHCl₃, respectively.

The hypsochromic shift in CHCl₃ can be understood by a combination of factors related to aggregation and polymer backbone deformation. A better solvation of polymer chains was observed in CHCl₃ than in hexane and it was postulated that CHCl₃ solvent molecules have stronger interaction with the conjugated backbone of the polymers than hexane molecules. DFT calculations showed the existence of C-H...X (where X = N, F, S) interactions of CHCl₃ molecules with the cyano groups of **P4-S** and fluorine atoms of **P4-F** (see **Figure 3** (a-d); H...X distances are in general smaller than the sum of van der Waals radii of H and X atoms).⁴⁷ These C-H...X interactions led to a loss of planarity in the backbone of different sized oligomers calculated for both **P4-S** and **P4-F** (see **Table S3** and **Figure S6**)

and, as a consequence, hypsochromic shifts were found for all of them when going from hexane solution to CHCl_3 solution (see Table S4). As an example, **Figure 3(e)** showed the blue shift calculated for the absorption spectra of tetramers of **P4-S** in CHCl_3 solution with respect to hexane (and for **P4-F** in **Figure S7**). Interestingly, the higher polarization effect induced by the malononitrile dithiolate in ssBTD subunits with respect to ffBTD, as indicated by the significantly larger computed dipole moment (7.64 D for ssBTD vs 3.02 D for ffBTD, see **Figure S8**) led to stronger interactions between CHCl_3 solvent molecules and **P4-S** backbone than in **P4-F**. The stabilization energy associated to the interaction of one CHCl_3 molecule with a monomer **P4-S** is 2.3 kcal mol⁻¹ higher (in absolute terms) than with a monomer **P4-F** (comparing the most stabilizing interactions of CHCl_3 molecule with both molecules; see **Figures S3** and **S4**). Accordingly, the hypsochromic shift calculated for the oligomers of **P4-S** is slightly larger than for those of **P4-F**, consistent with the experimental observations. In addition, the calculations show that the oligomer backbones of both **P4-S** and **P4-F** are more planar in hexane solution, which are conducive to a higher electronic coupling between monomer repeat units and, in consequence, may facilitate an “unconventional *J*-aggregate” according to exciton coupling theory,^{48,49} though the verification of this feature warrants future photophysical studies. Hexane solvent can also solubilize the polymers via strong interaction with the side chains and favors the polymer chains aggregation because the interaction between the non-polar hexane molecules and the polar polymer main chain is too weak to disentangle these chains.

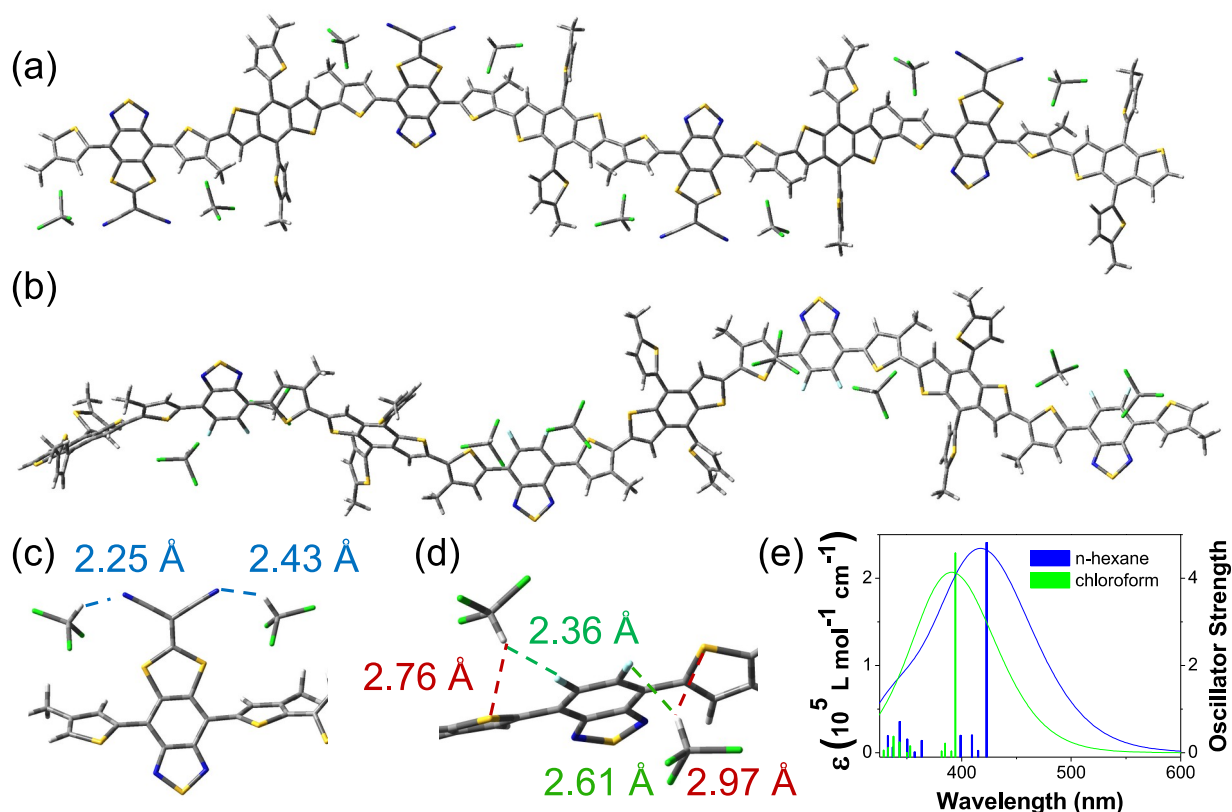


Figure 3. Tetrameric oligomers of (a) **P4-S** and (b) **P4-F** optimized in CHCl_3 solution (including both explicit and implicit solvent) at the $\omega\text{B97xD}/6\text{-31G}^{**}$ level of theory. Interactions between the (c) **P4-S** and (d) **P4-F** backbone and CHCl_3 solvent molecules. (e) Simulation of the hypochromic shift found for a tetramer **P4-S** going from hexane solution (blue trace) to CHCl_3 solution (green trace) at the TD- $\omega\text{B97xD}/6\text{-31G}^{**}$ level of theory (plotted with a peak half-width at half-height of 0.33 eV). The vertical bars correspond to the oscillator strengths of the calculated electronic transitions.

The solvent-dependent aggregation was further demonstrated by following the spectroscopic changes when introducing an antisolvent. As shown in **Figure 4a** and **4b**, two distinct phases were observed when adding different amount of MeOH into the CHCl_3 solution of **P4-S**.

Upon increasing the MeOH fraction, the absorption maximum of **P4-S** redshifted progressively until it reached a maximum wavelength at around 50% MeOH content, which

remained constant despite further increase of the MeOH fraction. This behavior corroborates antisolvent induced aggregation. While the polymer main chains are well solvated in CHCl_3 , leading to decreased chain coplanarity and weakened interchain interactions, the addition of MeOH promoted chain aggregation due to the repulsion between the alkyl chains and the polar solvent molecules, commensurate with a spectroscopic redshift. The plateaued peak position suggests that a saturated aggregated state is reached. Since both hexane and MeOH induce similar color changes, it supports that the solvation in hexane is primarily through interaction with the side chains rather than with the conjugated main chain, thus the polymer chains remain aggregated despite the alkyl “shell” being solvated. A superposition of absorption spectra of **P1**, **P3**, **P4-S** and **P4-F** in CHCl_3 indicates that **P1** is primarily aggregated even in CHCl_3 based on its broad, lower energy absorption feature, which is stark contrast to the other three polymers. This outlier suggests that linear side chains in **P1** strongly promotes the polymer chain aggregation such that the CHCl_3 -backbone interaction is severely screened. For the polymer **P2**, while its low solubility prevents a study in CHCl_3 , it can be dissolved in hot ODCB which allows for a variable temperature study by UV-vis spectroscopy (**Figure 4d**). An ODCB solution of polymer **P2** shows a broad absorption peak centered at 660 nm and an onset at around 850 nm at room temperature. At higher temperatures up to 180 °C, the absorption at 660 nm decreased together with the progressive blueshift of the onset, corresponding to a hypochromic shift of over 120 nm. The thermochromic changes are consistent with thermally induced polymer chain deaggregation, similar in nature as the solvatochromic behavior observed in **P4-S** and **P4-F**.

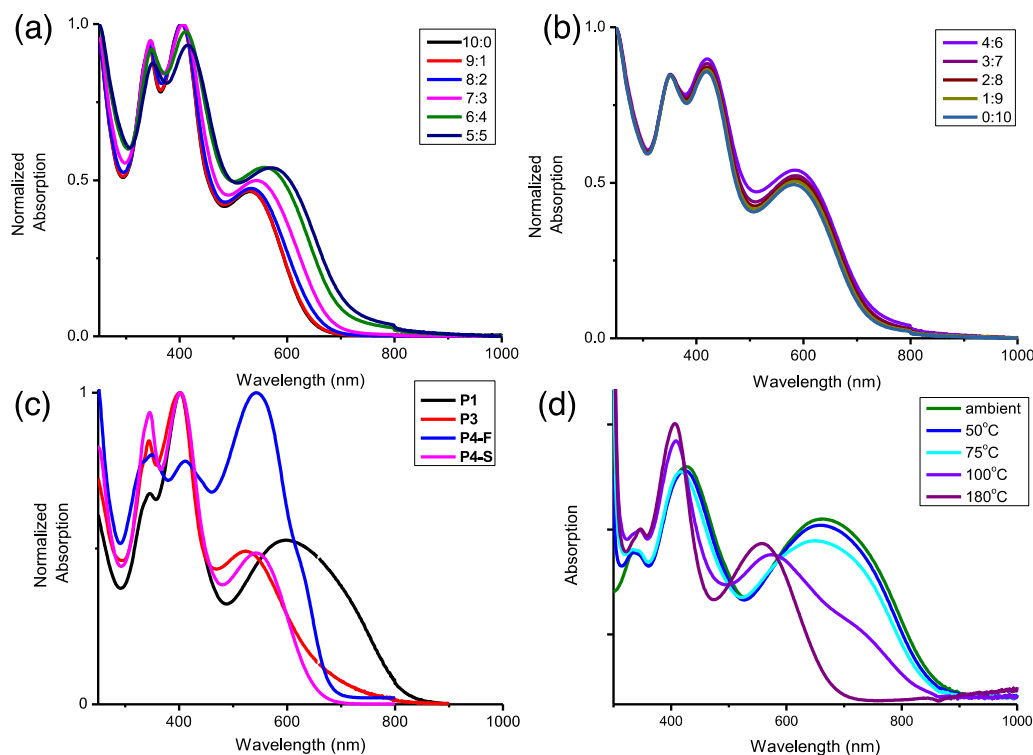


Figure 4. UV-vis spectra of **P4-S** in a mixture of CHCl₃:MeOH at different ratios: (a) from 10:10 to 6:4, and (b) from 5:5 to 0:10. (c) Comparison of UV-vis spectra of CHCl₃ solutions of **P1**, **P3**, **P4-S** and **P4-F**. (d) UV-vis spectra of **P2** in ODCB at different temperatures.

A final piece of evidence for aggregation-based chromatic behavior came from thin-film coatings of polymers **P4-S** and **P4-F**. Despite vastly different absorption spectra in chloroform and hexane solution, the thin films made from these solutions looked very similar, highly resembling the coloration of the aggregated hexane solution (**Figure S9**). There was slight peak broadening observed in the hexane deposited films, presumably due to an amount of pre-aggregation in solution that was grown upon during evaporation. As the deposited solution evaporated there were insufficient solvent molecules available to solubilize the polymer, causing a shift to the aggregated state regardless of which solvent was used to cast the film.

Electrochemical studies indicated that the **P4-S** has a LUMO energy of -3.59 eV, slightly higher than that of **P4-F** with -3.66 eV (**Table 3**). The HOMO level is notably higher than **P4-F** by 0.24 eV. Overall, dithioannulation has been effective in lowering both HOMO and LUMO energies of the BTD unit. In conjugated polymers, the thiolated **P4-S** shows more sensitive responses towards solvent and temperature than **P4-F**, due to more pronounced solvent-backbone interactions induced by the polar dithiolate substitution.

Morphological Studies. More insight of polymer aggregation behavior in the thin films were obtained from detailed grazing incidence wide angle X-ray scattering (GIWAXS) studies of the more soluble polymers **P4-S** and **P4-F**. Thin films of these polymers were obtained by spincoating their CHCl₃ solutions onto SiO₂/Si substrates, which were then placed on a heating stage situated in an Ar-purged chamber and analyzed by variable temperature GIWAXS. GIWAXS spectra were obtained while heating the polymer thin film samples up to 180 °C and cooling to 30 °C. As indicated by the in-plane and out-of-plane linecuts in **Figure 5a-d**, each polymer adopted a bimodal texture due to the presence of both face-on and edge-on oriented crystallites, with the face-on orientation being the predominant one persistent at all temperatures. As the temperature was increased, the 100 peak in the in-plane direction became significantly narrower (**Figure 5a** and **5c**), together with the appearance of higher order peaks, suggesting improved crystallinity of the face-on lamella with an increased crystallite size. There were minimal changes of *d*-spacings for the in-plane 100 peaks and out-of-plane 001 peaks upon annealing, in accordance with a constant inter-lamellar distance of 2.4 nm and π - π stacking distance of ~0.43 nm for the face-on crystallites of both polymers. The thermally induced crystallinity enhancement was more prominent in the case of **P4-S**, as

supported by the narrower 100 peak, the introduction of higher order peaks in the in-plane direction, and the much narrower 001 peak in the out-of-plane direction.

More information was also obtained for the edge-on crystallites. The out-of-plane 100 peaks of both polymers (**Figure 5b** and **5d**), corresponding to the lamella stacking normal to the substrate, showed a noticeable thermal induced contraction as indicated by the shift of such peaks towards larger q . The peak width remained quite broad, however, in sharp contrast to the in-plane 100 peaks. These results indicated that while thermal annealing had a more pronounced impact on interchain packing for the edge-on crystallites (more compact inter-lamellar packing) than the face-on ones, the crystallite size changes for these edge-on crystallites are much less notable than these for the face-on crystallites.

Upon cooling to close to room temperature, the high crystallinity remained, as indicated by the retention of the peak position and width. Such variable temperature studies revealed that for both **P4-S** and **P4-F**, the polymer chain conformations were thermally relaxed at higher temperature, facilitating the crystallization into more ordered crystallites. The irreversible crystallinity changes in thin films contrast with the reversible chain aggregation/disaggregation observed in solution. This observation also validates thermal annealing as an effective method to increase and lock-in the crystallinity of **P4-S** and **P4-F** in thin films, a welcoming feature for device optimization via thermal annealing. Furthermore, thermally treated **P4-S** was more crystalline than that of **P4-F**, as indicated by narrower peaks and more high order reflections in the overlay of their diffraction patterns (**Figure 5d** and **5e**).

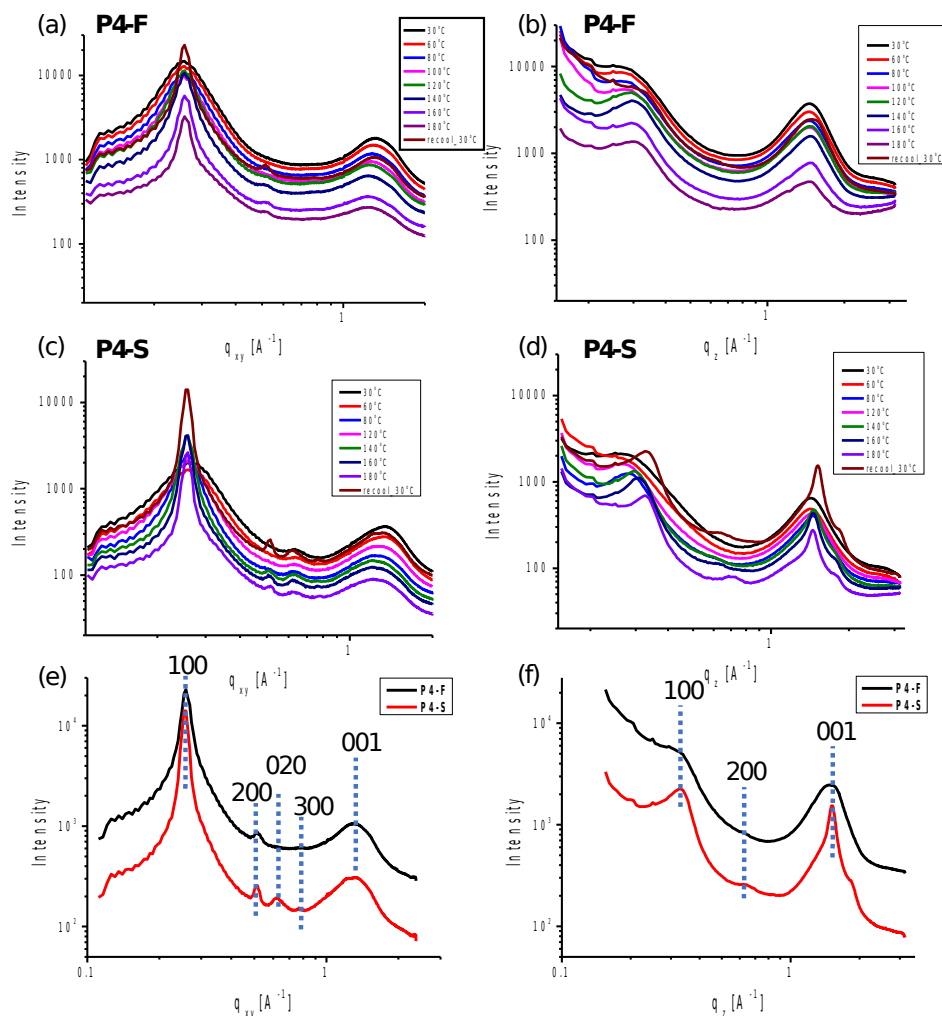


Figure 5. Linecuts of variable temperature GIWAXS of **P4-F** in the (a) in-plane and (b) out-of-plane directions, and linecuts of **P4-S** in the (c) in-plane and (d) out-of-plane directions. For direct comparison the patterns of fully annealed **P4-S** and **P4-F** were superimposed in the (e) in-plane and (f) out-of-plane directions.

In order to better understand the chain packing behavior, the crystal structures of both polymers were modeled by DFT calculations in periodic boundary conditions. We found that the π -stacked polymer chains were slipped in the backbone direction (~ 0.40 nm for **P4-S** and ~ 0.41 nm for **P4-F**) with respect to the cofacial arrangement (x-axis, according to **Figure 6**, **S10** and **S11**). The backbone of **P4-F** adopts a wavy shape probably due to steric hindrances between alkylthiophene-substituted BDT subunits (**Figure 6a**). The slipping along the x-axis

leads to π - π stacking interactions only in certain parts of **P4-F** backbone such that ffBTD subunits interact with thiophene subunits of neighboring chains with centroid-centroid distances of 0.43–0.51 nm (**Figure 6d**). Interestingly, the larger slip along the normal direction of backbone propagation (y-axis) found for **P4-S** with respect to **P4-F** (~ 0.43 nm for **P4-S** and ~ 0.17 nm for **P4-F**) reduces the steric hindrance and avoids bending of the chain backbone but also hampers π - π stacking interactions (**Figure 6b**). The **P4-S** three-dimensional structure is stabilized by electrostatic interactions between ssBTD subunits and thiophene subunits of neighboring chains (**Figure 6c**). Thus, the higher steric hindrances and backbone bending computed for **P4-F** and the differences found in the stabilizing interactions of both polymers could explain their distinct crystallinity.

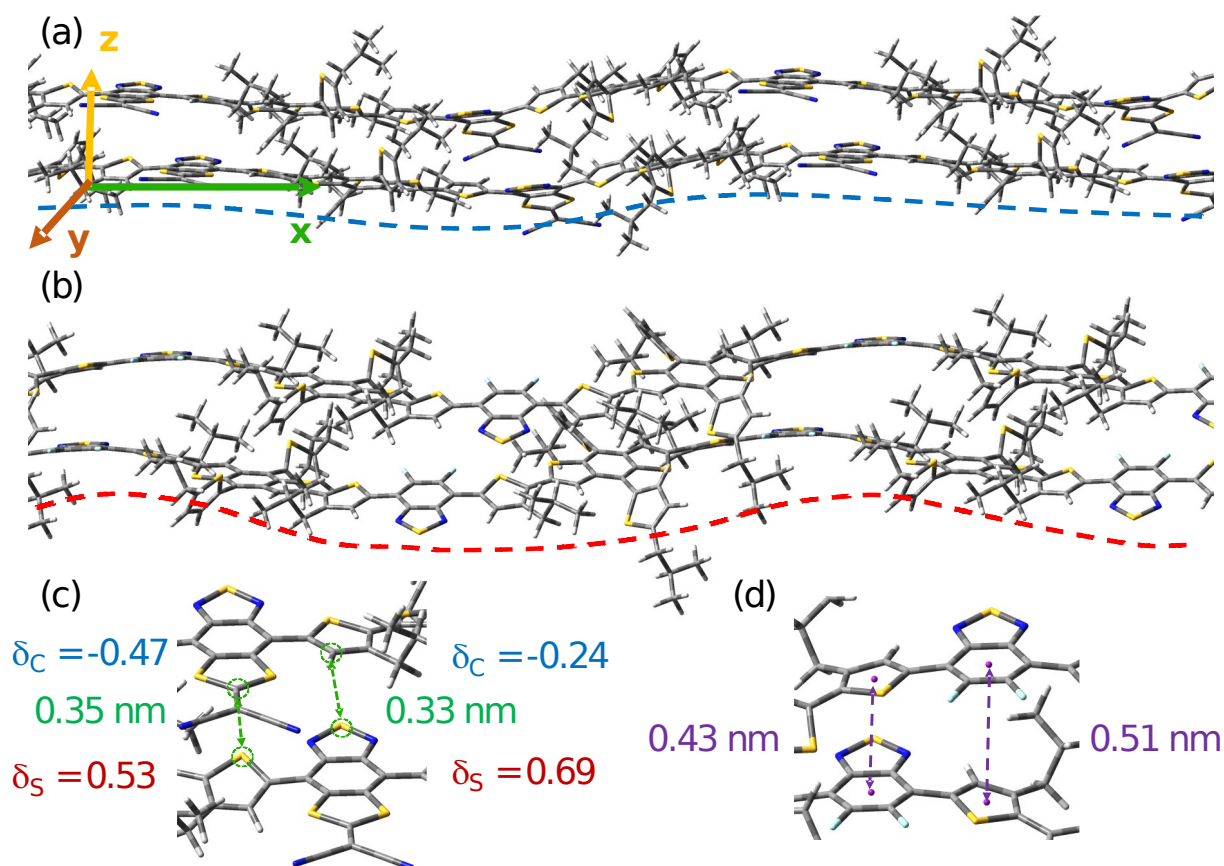


Figure 6. Two stacked polymer chains extracted from the three-dimensional structure calculated for (a) **P4-S** and (b) **P4-F** polymers at the HSE06/3-21G* level of theory. Dashed

lines indicate the polymer chain shape. (c) Some interchain S...C electrostatic interactions between ssBTD and thiophene subunits of **P4-S**. (d) Centroid-centroid distances between ffBTD and thiophene subunits from adjacent polymer chains of **P4-F**.

Incorporation of P4-S and P4-F into OFETs. **P4-F** was previously used as the active material for organic solar cells⁵⁰ and ffBTD-based polymers with similar structures were used for OFETs.^{51,52} Prior OFET studies suggested that despite their low lying LUMO levels, all ffBTD-based polymers behaved as *p*-type hole conductors. Herein both **P4-F** and **P4-S** were incorporated in OFETs and their carrier transport properties were compared side by side. Top gate bottom contact (TGBC) devices were fabricated on glass substrates, using PMMA as the dielectric layer, Au or Au-Cs₂CO₃ as the source/drain electrodes and Al as the gate electrode. The channel width and channel length were 4500 and 40 μm, respectively. *ortho*-Dichlorobenzene (ODCB) was chosen as the solvent for its ability to give continuous thin films with good coverage on the substrates. The active layers were deposited by spincoating into thin films from their respective ODCB solutions, followed by thermal annealing at 160 °C for 10 min. As shown in **Figure 7** and **Table 4**, **P4-F** showed a unipolar hole transport behavior, with an average mobility of 1.9E-3 cm² V⁻¹ s⁻¹. In contrast, **P4-S** displayed ambipolar transport characteristics. For the lower molecular weight **P4-S** extracted by hexane, it showed an average hole mobility of 2.4E-4 cm² V⁻¹ s⁻¹ and electron mobility of 3.0E-5 cm² V⁻¹ s⁻¹. The carrier mobilities were slightly lower in the case of THF-extracted **P4-S**, which displayed an average hole mobility of 1.3E-4 cm² V⁻¹ s⁻¹ and electron mobility of 2.2E-5 cm² V⁻¹ s⁻¹, respectively. Atomic force microscopic (AFM) studies revealed a root-mean-square roughness over 6 nm for each polymer thin film, which suggested large grain boundaries due to strong aggregation and may be accountable for the moderate mobilities (**Figure 8**). Despite

the lower hole mobility, the ambipolar behavior of **P4-S** suggests that the displacement of the difluoride functionality with the malonitrile dithiolate group effectively augments the electron transport, a feature rarely reported for ffBTD based polymers.

Table 4. Summary of OFET characteristics of **P4-S** and **P4-F**. The average mobilities were based on the test of 8-12 devices.

Polymers	$\mu_h^{\text{avg.a)}$ ($\text{cm}^2 \text{V}^{-1} \text{s}^{-1}$)	$\mu_h^{\text{max.b)}$ ($\text{cm}^2 \text{V}^{-1} \text{s}^{-1}$)	$V_{th, \text{hole}}$ (V)	$I_{\text{On}}/I_{\text{Off, hole}}$	$\mu_e^{\text{avg.c)}$ ($\text{cm}^2 \text{V}^{-1} \text{s}^{-1}$)	$\mu_e^{\text{max.d)}$ ($\text{cm}^2 \text{V}^{-1} \text{s}^{-1}$)	$V_{th, \text{elec}}$ (V)	$I_{\text{On}}/I_{\text{Off, elec}}$
P4-F	1.9×10^{-3}	2.1×10^{-3}	- 12 ± 1.5	10^4	-	-	-	-
P4-S-hexane	2.4×10^{-4}	2.6×10^{-4}	-30 ± 2	10^4	3.0×10^{-5}	3.5×10^{-5}	33 ± 2	10^4
P4-S-THF	1.3×10^{-4}	1.4×10^{-4}	-31 ± 2	10^4	2.2×10^{-5}	2.6×10^{-5}	34 ± 2	10^4

^{a)}average hole mobility; ^{b)}maximum hole mobility; ^{c)}average electron mobility; ^{d)}maximum hole mobility.

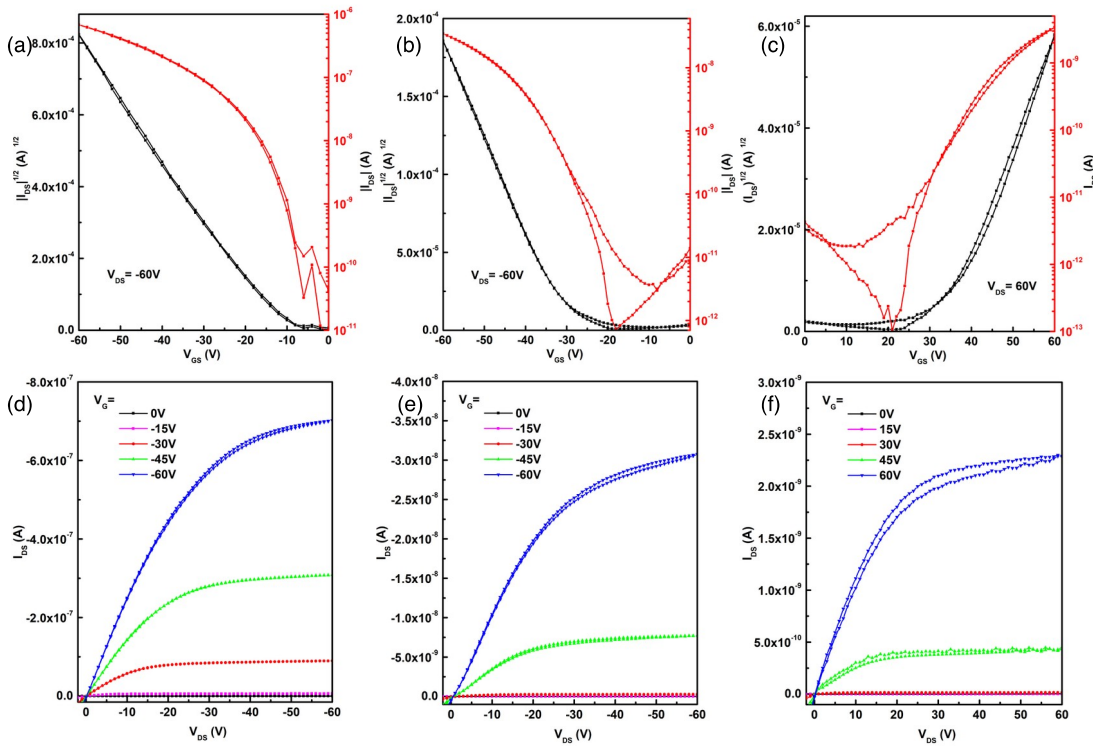


Figure 7. (a-c) Transfer and (d-f) output curves of (a) and (d) **P4-F** and (b), (c), (e) and (f) **P4-S**.

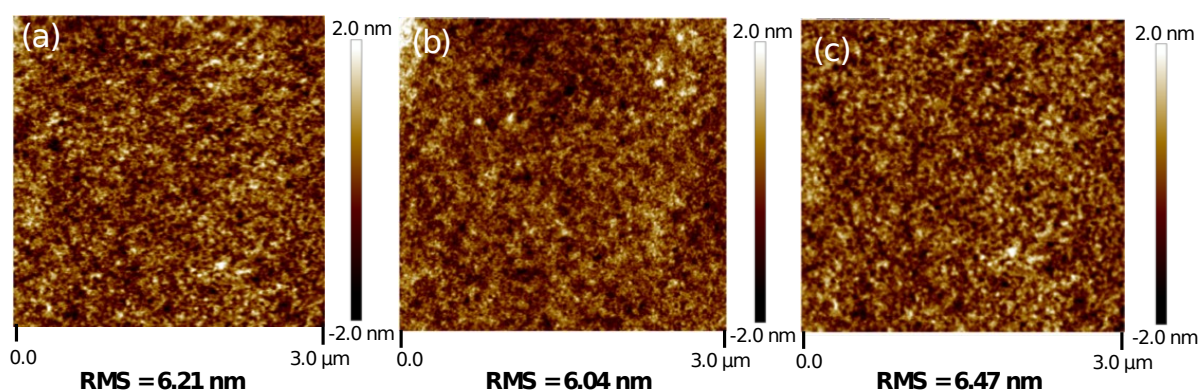


Figure 8. AFM height images of thin films of (a) **P4-F**, (b) **P4-S** from hexane, and (c) **P4-S** from THF.

Conclusions

This study provides the first assessment of a dithiolate substitution strategy for annulated BTD acceptors, including the synthesis of both small molecules and the related conjugated polymers, optical and electrical characterization of their solutions and thin films, and in-depth molecular level understanding by DFT calculations. The annulated ssBTD unit was synthesized via S_NAr displacement of fluorides in difluorobenzothiadiazole with the electron withdrawing 2-(1,3-dithiol-2-ylidene)malonitrile unit. Different from other known annulated BTD units, the introduction of the annulated dicyanomethylene dithiolate effectively lowers not only the LUMO energy level of the parent BTD, but also the HOMO energy level. Compared to the ffBTD counterpart, the thiolated ssBTD has a similar band gap, though the latter has exhibited more absorption features in the bluer region with higher

extinction coefficient. When ssBTD is incorporated into conjugated polymers, the resulting polymers show dramatic solvatochromatic and thermochromic responses in solution, which correlate well with the electronic effect and aggregation behavior imbued by the electron-deficient thiolation. Insight from theoretical modeling reveals that the thiolation induces a larger dipole moment and more pronounced interactions with polar solvent molecules, leading to conformational changes of the polymer conjugation backbone that contribute to the remarkable solvatochromism. Variable temperature GIWAXS studies of the polymer thin films indicated higher crystallinity in thermally treated **P4-S** compared to the ffBTD-based polymer **P4-F**. DFT modeling of three-dimensional polymer structures revealed that both electrostatic interactions and steric effects in ssBTD-based polymer **P4-S** contributed to the different chain packing motifs from those observed in **P4-F**. When incorporated in OFET devices, the ssBTD polymer **P4-S** behaves as an ambipolar semiconductor, in contrast to the hole-only transporting ffBTD-based **P4-F**. It is noted that the moderate mobilities may be a result of inferior crystallite domain sizes and boundaries, which could be further improved via side chain engineering. Collectively we have demonstrated that the thiolation method has a strong influence on the electronic properties of BTDs by impacting molecular energy levels, aggregation behavior, and ultimately the polarity of charge carriers in FET devices, validating the potential of thioannulated BTD as a versatile electron accepting unit for the design of functional stimuli-responsive optoelectronic materials.

Experimental Section

S1,⁵³ **1a**,⁵³ **1b**⁵⁰ and **2**⁵⁴ were synthesized according to literature methods. **1c** was purchased from Derthon Optoelectronic Materials Science Technology Co., Ltd.

3a: Difluoride **1a** (25 mg, 0.040 mmol) and **2** (10 mg, 0.056 mmol, 1.5 equiv.) were added to a vial with septa cap and stir bar which was then backfilled with nitrogen. DMF (2.0 mL) was added and the vial was placed in a 140 °C bath, quickly converting the yellow solution to brown. Once starting material was consumed as monitored by thin layer chromatography (TLC), the solution was diluted with dichloromethane, washed with water and brine before drying over MgSO₄. The crude reaction mixture was concentrated under reduced pressure and the residue was purified by column chromatography (gradient elution 0 to 25% dichloromethane in hexanes) to give the title compound as a bright orange solid (18 mg, 0.023 mmol, 58%). ¹H NMR (500 MHz, Chloroform-*d*) δ 7.51 (s, 2H), 7.28 (s, 2H), 2.73 (t, *J* = 7.8 Hz, 4H), 1.70 (t, *J* = 7.6 Hz, 4H), 1.26 (m, 36H), 0.88 (t, *J* = 6.8 Hz, 6H). ¹³C NMR (126 MHz, Chloroform-*d*) δ 177.4, 152.8, 144.5, 137.2, 135.0, 131.8, 124.7, 122.4, 112.4, 68.0, 32.1, 30.6, 30.6, 29.9, 29.9, 29.9, 29.8, 29.7, 29.6, 29.5, 22.9, 14.4. HRMS for C₄₂H₅₄N₄S₅ (MALDI): [M]⁺ Calcd: 774.2952, found 774.3621.

3b: Difluoride **1b** (509 mg, 0.910 mmol) and **2** (253 mg, 1.36 mmol, 1.5 equiv.) were added to a vial with septa cap and stir bar which was then backfilled with nitrogen. DMF (50 mL) was added and the vial was placed in a 140 °C bath, quickly converting the yellow solution to brown. After no further conversion as monitored by TLC (1.5 hrs) the solution was diluted with chloroform, washed with water and brine before drying over MgSO₄. The crude reaction mixture was concentrated under reduced pressure and the residue was purified by column chromatography (gradient elution 0 to 90% CHCl₃ in hexanes) to give the title compound as a bright orange solid (249 mg, 0.376 mmol, 41%). ¹H NMR (500 MHz, Chloroform-*d*) δ 7.49 (d, *J* = 1.4 Hz, 2H), 7.26 (d, *J* = 1.3 Hz, 2H), 2.74 – 2.62 (m, 4H), 1.63 (q, *J* = 6.1 Hz, 2H), 1.44 – 1.28 (m, 16H), 0.98 – 0.87 (m, 12H). ¹³C NMR (126 MHz, Chloroform-*d*) δ 177.2, 152.7, 143.0, 137.1, 134.9, 132.2, 125.6, 122.3, 112.3, 68.0, 40.6,

34.5, 32.7, 29.1, 25.7, 23.2, 14.4, 11.1. HRMS for $C_{34}H_{38}N_4S_5$ (MALDI): $[M]^+$ Calcd: 662.1700, found 662.2310.

4a: 3a (452 mg, 0.580 mmol) and *N*-bromosuccinimide (259 mg, 1.46 mmol, 2.5 equiv.) were added to a round-bottom flask with a stir bar which was then backfilled with nitrogen. Dichloromethane (24 mL) was added, followed by the addition of acetic acid (24 mL). The reaction was stirred overnight after which there was no starting material remaining as monitored by TLC. The reaction mixture was extracted 3 times with dichloromethane, washed with water (3x) and brine before drying over $MgSO_4$. The crude reaction mixture was concentrated under reduced pressure and the residue was purified by column chromatography (gradient elution 0 to 40% dichloromethane in hexanes) to give the title compound as a bright orange-red solid (465 mg, 0.500 mmol, 86%). 1H NMR (500 MHz, Chloroform-*d*) δ 7.38 (s, 2H), 2.68 (t, $J = 7.7$ Hz, 4H), 1.65 (p, $J = 7.9$ Hz, 4H), 1.44 – 1.21 (m, 36H), 0.93 – 0.84 (m, 6H). ^{13}C NMR (126 MHz, Chloroform-*d*) δ 176.5, 152.4, 143.3, 137.0, 134.8, 131.2, 121.5, 115.1, 112.2, 68.7, 32.2, 29.9, 29.9, 29.8, 29.6, 29.6, 29.4, 22.9, 14.4. HRMS for $C_{42}H_{52}Br_2N_4S_5$ (MALDI): $[M]^+$ Calcd: 930.1162, found 930.2996.

4b: 3b (174 mg, 0.260 mmol) and *N*-bromosuccinimide (117 mg, 0.660 mmol, 2.5 equiv.) were added to a round-bottom flask and stir bar, which was then backfilled with nitrogen. Dichloromethane (5 mL) was added, followed by the addition of acetic acid (5 mL). The reaction was stirred overnight after which there was no starting material remaining as confirmed by TLC. The reaction mixture was extracted 3 times with dichloromethane, washed with water (3x) and brine before drying over $MgSO_4$. The crude reaction mixture was concentrated under reduced pressure and the residue was purified by column chromatography (gradient elution 0 to 40% dichloromethane in hexanes) to give the title compound as a bright orange-red solid (160 mg, 0.195 mmol, 75%). 1H NMR (500 MHz, Chloroform-*d*) δ 7.35 (s, 2H), 2.72 – 2.52 (m, 4H), 1.76 – 1.62 (m, 2H), 1.44 – 1.18 (m, 16H), 1.03 – 0.81 (m, 12H).

^{13}C NMR (126 MHz, Chloroform-*d*) δ 176.3, 152.4, 142.4, 136.9, 134.7, 131.8, 121.5, 115.7, 112.2, 68.7, 40.1, 34.0, 32.7, 29.0, 25.8, 23.3, 14.4, 11.0. HRMS for $\text{C}_{30}\text{H}_{36}\text{Br}_2\text{F}_2\text{N}_2\text{S}_3$ (MALDI): $[\text{M}+\text{Na}]^+$ Calcd: 739.0268, found 739.0882.

4c: Difluoride **1c** (500 mg, 0.47 mmol) and **2** (110 mg, 0.59 mmol, 1.25 equiv.) were added to a vial with septa cap and stir bar which was then backfilled with nitrogen. DMF (2 mL) was added and the vial was placed in a 80 °C bath, quickly converting the yellow solution to brown. Once starting material was consumed in 1 hr, the solution was diluted with CHCl_3 , washed with ammonium chloride (aq), water, and brine before drying over MgSO_4 . The crude reaction mixture was concentrated under reduced pressure and purified by column chromatography (gradient elution 0 to 100% EtOAc in hexanes) to give the title compound as a bright orange-red solid (506 mg, 0.440 mmol, 93%). ^1H NMR (500 MHz, Chloroform-*d*) δ 7.36 (s, 2H), 2.61 (d, $J = 7.1$ Hz, 4H), 1.77 – 1.69 (m, 2H), 1.39 – 1.16 (m, 64H), 0.87 (t, $J = 6.8$ Hz, 12H). ^{13}C NMR (126 MHz, Chloroform-*d*) δ 176.1, 152.3, 142.5, 136.8, 134.6, 131.9, 121.4, 115.6, 112.1, 68.7, 38.7, 34.4, 33.5, 32.1, 30.2, 30.2, 29.9, 29.9, 29.8, 29.6, 29.6, 26.7, 22.9, 14.4. HRMS for $\text{C}_{58}\text{H}_{84}\text{Br}_2\text{N}_4\text{S}_5$ (MALDI): $[\text{M}]^+$ Calcd: 1154.3666, found 1154.5504.

P1: 4a (233 mg, 0.250 mmol, 1.0 equiv.), 2,5-bis(trimethylstannyl)thiophene **5** (102 mg, 0.250 mmol, 1.0 equiv.), $\text{Pd}_2(\text{dba})_3$ (4.8 mg, 0.0053 mmol, 0.021 equiv.), and tri(*o*-tolyl)phosphine (6.1 mg, 0.020 mmol, 0.080 equiv.) were added to an oven dried 50 mL 2-neck round-bottom flask with a reflux condenser and stir bar. Nitrogen gas was allowed to flow through the headspace for 30 mins. Dry xylene (11 mL) was added and the reaction was heated to 150 °C for 4 days, with an additional 5 mL xylene added after the first day due to solvent evaporation. Tributylstannyl thiophene (0.20 mL, 0.63 mmol) was added, followed by 2-bromothiophene (0.20 mL, 0.63 mmol) after 4 hrs. At the following day, the reaction mixture was concentrated and precipitated into methanol (100 mL). The polymer was

purified via sequential Soxhlet extraction with methanol, acetone, hexanes, dichloromethane, CHCl_3 , and chlorobenzene.

P2: 4a (100 mg, 0.107 mmol, 1.0 equiv.), 5,5'-bis(trimethylstannyl)-2,2'-bithiophene **6** (52.7 mg, 0.107 mmol, 1.0 equiv.), $\text{Pd}_2(\text{dba})_3$ (2.1 mg, 0.0022 mmol, 0.021 equiv.), and tri(o-tolyl)phosphine (2.6 mg, 0.0086 mmol, 0.080 equiv.) were added to a vial with septa cap and stir bar. Nitrogen gas was allowed to flow through the headspace for 30 mins. Dry xylene (2 mL) was added and the reaction was heated to 150 °C for 4 days, with an additional 2 mL xylene added after the second day due to solvent evaporation. Tributylstannyl thiophene (0.10 mL, 0.32 mmol) was added, followed by 2-bromothiophene (0.10 mL, 0.32 mmol) after 4 hrs. At the following day, the reaction mixture was concentrated and precipitated into methanol. The polymer was purified via sequential Soxhlet extraction with methanol, acetone, hexanes, dchloromethane, CHCl_3 , and chlorobenzene.

P3: 4b (76 mg, 0.16 mmol, 1.0 equiv.), 2,5-bis(trimethylstannyl)thieno[3,2-b]thiophene **7** (134 mg, 0.16 mmol, 1.0 equiv.), $\text{Pd}_2(\text{dba})_3$ (3.1 mg, 0.0034 mmol, 0.021 equiv.), and tri(o-tolyl)phosphine (4.0 mg, 0.013 mmol, 0.080 equiv.) were added to an oven dried 50 mL 2-neck round-bottom flask with a reflux condenser and stir bar. Nitrogen gas was allowed to flow through the headspace for 30 mins. Dry xylene (11 mL) was added and the reaction was heated to 150 °C for 4 days, with an additional 5 mL xylene added after the third day due to solvent evaporation. Tributylstannyl thiophene (0.20 mL, 0.63 mmol) was added followed by 2-bromothiophene (0.20 mL, 0.63 mmol) after 4 hrs. At the following day, the reaction mixture was concentrated and precipitated into methanol (100 mL). The polymer was purified via sequential Soxhlet extraction with methanol, acetone, hexanes, dichloromethane, CHCl_3 , and chlorobenzene.

P4-F: 1c (183 mg, 0.173 mmol, 1.0 equiv.) and (4,8-bis(5-(2-ethylhexyl)thiophen-2-yl)benzo[1,2-b:4,5-b']dithiophene-2,6-diyl)bis(trimethylstannane) **8** (156 mg, 0.173 mmol, 1

equiv.) were added to an oven dried 50 mL 2-neck round-bottom flask with a reflux condenser and stir bar. The system was backfilled four times with nitrogen gas and dry toluene (12 mL) was added. The solution was sparged with nitrogen for 15 mins before Pd(PPh₃)₄ (15 mg, 0.013 mmol, 0.075 equiv.) was added. The solution was sparged with nitrogen for an additional 10 mins before being placed in a 90°C bath. After 3 days the reaction was concentrated and precipitated into methanol. An attempt was made to purify the polymer via Soxhlet extraction but it was completely soluble in hot hexanes.

P4-S: **4c** (200 mg, 0.173 mmol, 1.0 equiv.) and (4,8-bis(5-(2-ethylhexyl)thiophen-2-yl)benzo[1,2-b:4,5-b']dithiophene-2,6-diyl)bis(trimethylstannane) **8** (156 mg, 0.173 mmol, 1.0 equiv.) were added to an oven dried 50 mL 2-neck round-bottom flask with a reflux condenser and stir bar. The system was backfilled four times with nitrogen gas and dry toluene (12 mL) was added. The solution was sparged with nitrogen for 15 mins before Pd(PPh₃)₄ (15 mg, 0.013 mmol, 0.075 equiv.) was added. The solution was sparged with nitrogen for an additional 10 mins before being placed in a 90 °C bath. After 3 days the reaction was concentrated and precipitated into methanol. The polymer was fractionated via sequential Soxhlet extraction with hexanes and THF.

Supporting Information

The Supporting Information is available free of charge on the ACS Publications website.

Additional experimental details, computational details, figures and tables on conformational analysis, frontier molecular orbitals, and optical transitions, TGA and DSC curves, NMR spectra (PDF)

Conflicts of interest

There are no conflicts to declare.

Acknowledgements

This work was conducted at the Molecular Foundry, Lawrence Berkeley National Laboratory, and GIWAXS data was collected at BL7.3.3 at Advanced Light Source, both being supported by the Office of Science, Office of Basic Energy Sciences, of the U.S. Department of Energy under Contract No. DE-AC02-05CH11231. The authors would like to thank the ‘Consejería de Economía y Conocimiento. Junta de Andalucía’ (FQM-337) for supporting this research. The authors thank ‘Centro de Servicios de Informática y Redes de Comunicaciones’ (CSIRC) (Universidad de Granada, Spain) for providing the computing time.

References

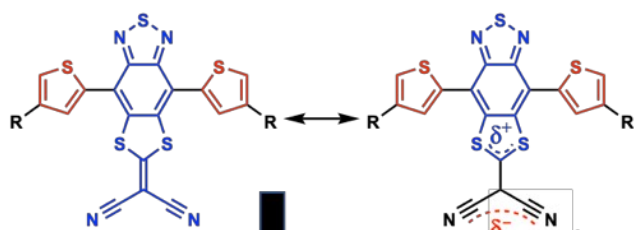
- (1) Bronstein, H.; Nielsen, C. B.; Schroeder, B. C.; McCulloch, I. The Role of Chemical Design in the Performance of Organic Semiconductors. *Nat. Rev. Chem.* **2020**, *4*, 66-77.
- (2) Wang, C.; Dong, H.; Hu, W.; Liu, Y.; Zhu, D. Semiconducting Π -Conjugated Systems in Field-Effect Transistors: A Material Odyssey of Organic Electronics. *Chem. Rev.* **2011**, *112*, 2208-2267.
- (3) Mei, J.; Diao, Y.; Appleton, A. L.; Fang, L.; Bao, Z. Integrated Materials Design of Organic Semiconductors for Field-Effect Transistors. *J. Am. Chem. Soc.* **2013**, *135*, 6724-6746.
- (4) Dong, H.; Fu, X.; Liu, J.; Wang, Z.; Hu, W. 25th Anniversary Article: Key Points for High-Mobility Organic Field-Effect Transistors. *Adv. Mater.* **2013**, *25*, 6158-6183.
- (5) Li, H.; Kim, F. S.; Ren, G.; Jenekhe, S. A. High-Mobility N-Type Conjugated Polymers Based on Electron-Deficient Tetraazabenzodifluoranthene Diimide for Organic Electronics. *J. Am. Chem. Soc.* **2013**, *135*, 14920-14923.
- (6) Zhao, Y.; Guo, Y.; Liu, Y. 25th Anniversary Article: Recent Advances in N-Type and Ambipolar Organic Field-Effect Transistors. *Adv. Mater.* **2013**, *25*, 5372-5391.
- (7) Cai, Z.; Luo, H.; Qi, P.; Wang, J.; Zhang, G.; Liu, Z.; Zhang, D. Alternating Conjugated Electron Donor–Acceptor Polymers Entailing Pechmann Dye Framework as the Electron Acceptor Moieties for High Performance Organic Semiconductors with Tunable Characteristics. *Macromolecules* **2014**, *47*, 2899-2906.
- (8) Takeda, Y.; Andrew, T. L.; Lobe, J. M.; Mork, A. J.; Swager, T. M. An Air-Stable Low-Bandgap N-Type Organic Polymer Semiconductor Exhibiting Selective Solubility in Perfluorinated Solvents. *Angew. Chem. Int. Ed.* **2012**, *51*, 9042-9046.
- (9) Lei, T.; Xia, X.; Wang, J.-Y.; Liu, C.-J.; Pei, J. “Conformation Locked” Strong Electron-Deficient Poly(P-Phenylene Vinylene) Derivatives for Ambient-Stable N-Type Field-Effect Transistors: Synthesis, Properties, and Effects of Fluorine Substitution Position. *J. Am. Chem. Soc.* **2014**, *136*, 2135-2141.
- (10) Inganäs, O. Organic Photovoltaics over Three Decades. *Adv. Mater.* **2018**, *30*, 1800388.
- (11) Li, Y.; Yao, K.; Yip, H.-L.; Ding, F.-Z.; Xu, Y.-X.; Li, X.; Chen, Y.; Jen, A. K. Y. Eleven-Membered Fused-Ring Low Band-Gap Polymer with Enhanced Charge Carrier Mobility and Photovoltaic Performance. *Adv. Funct. Mater.* **2014**, *24*, 3631-3638.
- (12) Thompson, B. C.; Frechet, J. M. J. Polymer-Fullerene Composite Solar Cells. *Angew. Chem. Int. Ed.* **2008**, *47*, 58-77.

- (13) Brus, V. V.; Lee, J.; Luginbuhl, B.; Ko, S.-J.; Bazan, G. C.; Nguyen, T.-Q. Solution-Processed Semitransparent Organic Photovoltaics: From Molecular Design to Device Performance. *Adv. Mater.* **2019**, *31*, 1970219.
- (14) Wang, C.; Fu, B.; Zhang, X.; Li, R.; Dong, H.; Hu, W. Solution-Processed, Large-Area, Two-Dimensional Crystals of Organic Semiconductors for Field-Effect Transistors and Phototransistors. *ACS Cent. Sci.* **2020**, *6*, 636-652.
- (15) D'Andrade, B. W.; Forrest, S. R. White Organic Light-Emitting Devices for Solid-State Lighting. *Adv. Mater.* **2004**, *16*, 1585-1595.
- (16) Huang, Y.; Elder, D. L.; Kwiram, A. L.; Jenekhe, S. A.; Jen, A. K. Y.; Dalton, L. R.; Luscombe, C. K. Organic Semiconductors at the University of Washington: Advancements in Materials Design and Synthesis and toward Industrial Scale Production. *Adv. Mater.* **2019**, Ahead of Print.
- (17) Beaujuge, P. M.; Reynolds, J. R. Color Control in Π -Conjugated Organic Polymers for Use in Electrochromic Devices. *Chem. Rev.* **2010**, *110*, 268-320.
- (18) Chaudhary, A.; Pathak, D. K.; Tanwar, M.; Yogi, P.; Sagdeo, P. R.; Kumar, R. Polythiophene-Pcbm-Based All-Organic Electrochromic Device: Fast and Flexible. *ACS Appl. Electron. Mater.* **2019**, *1*, 58-63.
- (19) He, J.; You, L.; Tran, D. T.; Mei, J. Low-Temperature Thermally Annealed Niobium Oxide Thin Films as a Minimally Color Changing Ion Storage Layer in Solution-Processed Polymer Electrochromic Devices. *ACS Appl. Mater. Interfaces* **2019**, *11*, 4169-4177.
- (20) Takimiya, K.; Osaka, I.; Nakano, M. Π -Building Blocks for Organic Electronics: Reevaluation of "Inductive" and "Resonance" Effects of Π -Electron Deficient Units. *Chem. Mater.* **2013**, *26*, 587-593.
- (21) Wang, Y.; Michinobu, T. Benzothiadiazole and Its Π -Extended, Heteroannulated Derivatives: Useful Acceptor Building Blocks for High-Performance Donor-Acceptor Polymers in Organic Electronics. *J. Mater. Chem. C* **2016**, *4*, 6200-6214.
- (22) Parker, T. C.; Patel, D. G.; Moudgil, K.; Barlow, S.; Risko, C.; Brédas, J.-L.; Reynolds, J. R.; Marder, S. R. Heteroannulated Acceptors Based on Benzothiadiazole. *Mater. Horiz.* **2015**, *2*, 22-36.
- (23) Tam, T. L.; Li, H.; Lam, Y. M.; Mhaisalkar, S. G.; Grimsdale, A. C. Synthesis and Characterization of [1,2,5]Chalcogenazolo[3,4-F]Benzo[1,2,3]Triazole and [1,2,3]Triazolo[3,4-G]Quinoxaline Derivatives. *Org. Lett.* **2011**, *13*, 4612-4615.
- (24) Keshtov, M. L.; Kuklin, S. A.; Radychev, N. A.; Nikolaev, A. Y.; Ostapov, I. E.; Krayushkin, M. M.; Konstantinov, I. O.; Koukaras, E. N.; Sharma, A.; Sharma, G. D. New Low Bandgap near-Ir Conjugated D-a Copolymers for Bhj Polymer Solar Cell Applications. *Phys. Chem. Chem. Phys.* **2016**, *18*, 8389-8400.
- (25) Keshtov, M. L.; Kuklin, S. A.; Radychev, N. A.; Nikolaev, A. Y.; Koukaras, E. N.; Sharma, A.; Sharma, G. D. Design and Synthesis of New Ultra-Low Band Gap Thiadiazoloquinoxaline-Based Polymers for near-Infrared Organic Photovoltaic Application. *RSC Advances* **2016**, *6*, 14893-14908.
- (26) Qi, J.; Qiao, W.; Wang, Z. Y. Advances in Organic near-Infrared Materials and Emerging Applications. *Chem. Rec.* **2016**, *16*, 1531-1548.
- (27) Hu, X.; Dong, Y.; Huang, F.; Gong, X.; Cao, Y. Solution-Processed High-Detectivity near-Infrared Polymer Photodetectors Fabricated by a Novel Low-Bandgap Semiconducting Polymer. *J. Phys. Chem. C* **2013**, *117*, 6537-6543.
- (28) Patel, D. G.; Feng, F.; Ohnishi, Y.-y.; Abboud, K. A.; Hirata, S.; Schanze, K. S.; Reynolds, J. R. It Takes More Than an Imine: The Role of the Central Atom on the Electron-Accepting Ability of Benzotriazole and Benzothiadiazole Oligomers. *J. Am. Chem. Soc.* **2012**, *134*, 2599-2612.
- (29) Lee, J.; Jang, M.; Lee, S. M.; Yoo, D.; Shin, T. J.; Oh, J. H.; Yang, C. Fluorinated Benzothiadiazole (Bt) Groups as a Powerful Unit for High-Performance Electron-Transporting Polymers. *ACS Appl. Mater. Interfaces* **2014**, *6*, 20390-20399.
- (30) Ragni, R.; Punzi, A.; Babudri, F.; Farinola, G. M. Organic and Organometallic Fluorinated Materials for Electronics and Optoelectronics: A Survey on Recent Research. *Eur. J. Org. Chem.* **2018**, *2018*, 3500-3519.
- (31) Olla, T.; Ibraikulov, O. A.; Ferry, S.; Boyron, O.; Mery, S.; Heinrich, B.; Heiser, T.; Leveque, P.; Leclerc, N. Benzothiadiazole Halogenation Impact in Conjugated Polymers, a Comprehensive Study. *Macromolecules* **2019**, *52*, 8006-8016.

- (32) Zhong, X.; Chen, H.; Wang, M.; Gan, S.; He, Q.; Chen, W.; He, F. Synergistic Effect of Chlorination and Selenophene: Achieving Elevated Solar Conversion in Highly Aggregated Systems. *Macromolecules* **2019**, *52*, 2393-2401.
- (33) Xu, B.; Pelse, I.; Agarkar, S.; Ito, S.; Zhang, J.; Yi, X.; Chujo, Y.; Marder, S.; So, F.; Reynolds, J. R. Randomly Distributed Conjugated Polymer Repeat Units for High-Efficiency Photovoltaic Materials with Enhanced Solubility and Processability. *ACS Appl. Mater. Interfaces* **2018**, *10*, 44583-44588.
- (34) Chen, S.; Wang, Y.; Zhang, L.; Zhao, J.; Chen, Y.; Zhu, D.; Yao, H.; Zhang, G.; Ma, W.; Friend, R. H.; Chow, P. C. Y.; Gao, F.; Yan, H. Efficient Non-Fullerene Organic Solar Cells with Small Driving Forces for Both Hole and Electron Transfer. *Adv. Mater.* **2018**, *30*, e1804215.
- (35) Mas-Montoya, M.; Li, J.; Wienk, M. M.; Meskers, S. C. J.; Janssen, R. A. J. Effects of Fluorination and Thermal Annealing on Charge Recombination Processes in Polymer Bulk-Heterojunction Solar Cells. *J. Mater. Chem. A* **2018**, *6*, 19520-19531.
- (36) Nketia-Yawson, B.; Jung, A. R.; Nguyen, H. D.; Lee, K.-K.; Kim, B.; Noh, Y.-Y. Difluorobenzothiadiazole and Selenophene-Based Conjugated Polymer Demonstrating an Effective Hole Mobility Exceeding $5 \text{ cm}^2 \text{ V}^{-1} \text{ s}^{-1}$ with Solid-State Electrolyte Dielectric. *ACS Appl. Mater. Interfaces* **2018**, *10*, 32492-32500.
- (37) Weng, K.; Xue, X.; Qi, F.; Zhang, Y.; Huo, L.; Zhang, J.; Wei, D.; Wan, M.; Sun, Y. Synergistic Effects of Fluorination and Alkylthiolation on the Photovoltaic Performance of the Poly(Benzodithiophene-Benzothiadiazole) Copolymers. *ACS Appl. Energy Mater.* **2018**, *1*, 4686-4694.
- (38) Ibraikulov, O. A.; Ngov, C.; Chavez, P.; Bulut, I.; Heinrich, B.; Boyron, O.; Gerasimov, K. L.; Ivanov, D. A.; Swaraj, S.; Mery, S.; Leclerc, N.; Leveque, P.; Heiser, T. Face-on Orientation of Fluorinated Polymers Conveyed by Long Alkyl Chains: A Prerequisite for High Photovoltaic Performances. *J. Mater. Chem. A* **2018**, *6*, 12038-12045.
- (39) Casey, A.; Han, Y.; Fei, Z.; White, A. J. P.; Anthopoulos, T. D.; Heeney, M. Cyano Substituted Benzothiadiazole: A Novel Acceptor Inducing N-Type Behaviour in Conjugated Polymers. *J. Mater. Chem. C* **2015**, *3*, 265-275.
- (40) Casey, A.; Green, J. P.; Shakya Tuladhar, P.; Kirkus, M.; Han, Y.; Anthopoulos, T. D.; Heeney, M. Cyano Substituted Benzotriazole Based Polymers for Use in Organic Solar Cells. *J. Mater. Chem. A* **2017**, *5*, 6465-6470.
- (41) Kim, H. S.; Song, C. E.; Ha, J.-W.; Lee, S.; Rasool, S.; Lee, H. K.; Shin, W. S.; Hwang, D.-H. Synthesis of Itic Derivatives with Extended π -Conjugation as Non-Fullerene Acceptors for Organic Solar Cells. *ACS Appl. Mater. Interfaces* **2019**, *11*, 47121-47130.
- (42) Yamashita, Y.; Suzuki, T.; Saito, G.; Mukai, T. Novel Quinone-Type Acceptors Fused with Sulphur Heterocycles and Their Highly Conductive Complexes with Electron Donors. *J. Chem. Soc., Chem. Commun.* **1986**, 1489-1491.
- (43) Gao, X.; Di, C.-a.; Hu, Y.; Yang, X.; Fan, H.; Zhang, F.; Liu, Y.; Li, H.; Zhu, D. Core-Expanded Naphthalene Diimides Fused with 2-(1,3-Dithiol-2-Ylidene)Malonitrile Groups for High-Performance, Ambient-Stable, Solution-Processed N-Channel Organic Thin Film Transistors. *J. Am. Chem. Soc.* **2010**, *132*, 3697-3699.
- (44) Luo, H.; He, D.; Zhang, Y.; Wang, S.; Gao, H.; Yan, J.; Cao, Y.; Cai, Z.; Tan, L.; Wu, S.; Wang, L.; Liu, Z. Synthesis of Heterocyclic Core-Expanded Bis-Naphthalene Tetracarboxylic Diimides. *Org. Lett.* **2019**, *21*, 9734-9737.
- (45) Zhang, F.; Hu, Y.; Schuettfort, T.; Di, C.-a.; Gao, X.; McNeill, C. R.; Thomsen, L.; Mannsfeld, S. C. B.; Yuan, W.; Sirringhaus, H.; Zhu, D. Critical Role of Alkyl Chain Branching of Organic Semiconductors in Enabling Solution-Processed N-Channel Organic Thin-Film Transistors with Mobility of up to $3.50 \text{ cm}^2 \text{ V}^{-1} \text{ s}^{-1}$. *J. Am. Chem. Soc.* **2013**, *135*, 2338-2349.
- (46) Zhao, Z.; Zhang, F.; Hu, Y.; Wang, Z.; Leng, B.; Gao, X.; Di, C.-a.; Zhu, D. Naphthalenediimides Fused with 2-(1,3-Dithiol-2-Ylidene)Acetonitrile: Strong Electron-Deficient Building Blocks for High-Performance N-Type Polymeric Semiconductors. *Acs Macro Lett* **2014**, *3*, 1174-1177.
- (47) Batsanov, S. S. Van Der Waals Radii of Elements. *Inorg. Mater.* **2001**, *37*, 871-885.

- (48) Spano, F. C.; Silva, C. H- and J-Aggregate Behavior in Polymeric Semiconductors. *Annu. Rev. Phys. Chem.* **2014**, *65*, 477-500.
- (49) Eder, T.; Stangl, T.; Gmelch, M.; Remmerssen, K.; Laux, D.; Höger, S.; Lupton, J. M.; Vogelsang, J. Switching between H- and J-Type Electronic Coupling in Single Conjugated Polymer Aggregates. *Nat. Commun.* **2017**, *8*, 1641.
- (50) Wang, N.; Chen, Z.; Wei, W.; Jiang, Z. Fluorinated Benzothiadiazole-Based Conjugated Polymers for High-Performance Polymer Solar Cells without Any Processing Additives or Post-Treatments. *J. Am. Chem. Soc.* **2013**, *135*, 17060-17068.
- (51) Liang, X.; Sun, W.; Chen, Y.; Tan, L.; Cai, Z.; Liu, Z.; Wang, L.; Li, J.; Chen, W.; Dong, L. A Vinyl Flanked Difluorobenzothiadiazole-Dithiophene Conjugated Polymer for High Performance Organic Field-Effect Transistors. *J. Mater. Chem. C* **2018**, *6*, 1774-1779.
- (52) Li, Z.; Lu, J.; Tse, S.-C.; Zhou, J.; Du, X.; Tao, Y.; Ding, J. Synthesis and Applications of Difluorobenzothiadiazole Based Conjugated Polymers for Organic Photovoltaics. *J. Mater. Chem.* **2011**, *21*, 3226-3233.
- (53) Wang, Y.; Xin, X.; Lu, Y.; Xiao, T.; Xu, X.; Zhao, N.; Hu, X.; Ong, B. S.; Ng, S. C. Substituent Effects on Physical and Photovoltaic Properties of 5,6-Difluorobenzo[C][1,2,5]Thiadiazole-Based D-a Polymers: Toward a Donor Design for High Performance Polymer Solar Cells. *Macromolecules* **2013**, *46*, 9587-9592.
- (54) Hatchard, W. R. The Synthesis of Isothiazoles. I. 3,5-Dichloro-4-Isothiazolecarbonitrile and Its Derivatives. *J. Org. Chem.* **1964**, *29*, 660-665.

Dithiolate annulated BTD



- Solvatochromic
- Thermochromic
- Ambipolar

